Current Topics

Structural and Dynamic Basis of Phospholamban and Sarcolipin Inhibition of Ca^{2+}-ATPase†

Nathaniel J. Traaseth,‡ Kim N. Ha,‡ Raffaello Verardi,§ Lei Shi,‡ Jarrod J. Buffy,§ Larry R. Masterson,‡ and Gianluigi Veglia*,‡,§

Department of Chemistry and Department of Biochemistry, Molecular Biology, and Biophysics, University of Minnesota, Minneapolis, Minnesota 55455

Received August 17, 2007; Revised Manuscript Received October 16, 2007

ABSTRACT: Phospholamban (PLN) and sarcolipin (SLN) are two single-pass membrane proteins that regulate Ca^{2+}-ATPase (SERCA), an ATP-driven pump that translocates calcium ions into the lumen of the sarcoplasmic reticulum, initiating muscle relaxation. Both proteins bind SERCA through intramembrane interactions, impeding calcium translocation. While phosphorylation of PLN at Ser-16 and/or Thr-17 reestablishes calcium flux, the regulatory mechanism of SLN remains elusive. SERCA has been crystallized in several different states along the enzymatic reaction coordinates, providing remarkable mechanistic information; however, the lack of high-resolution crystals in the presence of PLN and SLN limits the current understanding of the regulatory mechanism. This brief review offers a survey of our hybrid structural approach using solution and solid-state NMR methodologies to understand SERCA regulation from the point of view of PLN and SLN. These results have improved our understanding of the calcium translocation process and are the basis for designing new therapeutic approaches to ameliorate muscle malfunctions.

Two membrane proteins, sarco(endo)plasmic reticulum calcium ATPase (SERCA)[1] and the ryanodine receptors (Ryr), play major roles in calcium regulation within muscle cells. Ryr1 and Ryr2 are responsible for releasing Ca^{2+} from the sarcoplasmic reticulum (SR) of skeletal and cardiac muscle, respectively, resulting in muscle contraction. SERCA1a and SERCA2a pump calcium from the cytosol into the SR in skeletal and cardiac muscle, respectively, initiating muscle relaxation. Phospholamban (PLN), a 52-residue protein spanning the SR membrane (*1*), is an endogenous inhibitor of SERCA, lowering the apparent calcium affinity of the ATPase. The relief of SERCA inhibition is achieved by phosphorylation of PLN at Ser-16 by protein kinase A and/or Thr-17 by Ca^{2+}/calmodulin-dependent protein kinase (*2*). In vivo studies demonstrate that PLN phosphorylation at Ser-16 and Thr-17 has different physiological effects, suggesting that these mechanisms act independently (*3*, *4*).

Sarcolipin (SLN) has a primary sequence homologous to that of the transmembrane domain of PLN (*5*, *6*). Initially, SLN was thought to be the counterpart of PLN within skeletal muscle, playing only an ancillary role in cardiac muscle. Recently, however, significant expression levels of SLN have been detected in cardiac atrial muscle, with lower levels in ventricular muscle (*7*−*9*), suggesting that it may play an important role in regulation of the heart. When SLN was initially copurified with fast-twitch skeletal SERCA1a (*10*), no post-translational modifications were identified, which led to the conclusion that the regulation of SLN depended on its variable expression levels (*11*, *12*). Recent evidence shows that SLN inhibition can be fully reversed by isoproterenol, a β-adrenergic receptor agonist in PLN knockout mice (*13*). These results led to the hypothesis that the inhibitory effect of SLN can be reversed via phosphorylation in a manner similar to that of PLN. In vitro experiments have shown that SLN can be phosphorylated at Thr-5 when cotransfected with serine/threonine kinase 16 (STK16) (*13*). From these biological data, it is clear that phosphorylation of PLN and SLN constitute driving forces for calcium re-uptake into cardiac SR.

Several crystal structures of SERCA in different conformations within the enzymatic cycle have revealed important atomic details regarding SERCA's mechanism (Figure 1) (*14*−*19*). PLN is thought to bind and inhibit the low-affinity calcium form of SERCA (E2) and detach from the enzyme (either partially or totally) upon phosphorylation at Ser-16, reversing its inhibitory effect and restoring the affinity of SERCA for Ca^{2+} ions. The only experimental structure of

† This work was supported by grants to G.V. (NIH Grant GM64742, NIH Grant HL80081, and AHA Grant 0160465Z).

* To whom correspondence should be addressed: Department of Chemistry, University of Minnesota, 207 Pleasant St. S.E., Minneapolis, MN 55455. Telephone: (612) 625-0758. Fax: (612) 626-7541. E-mail: veglia@chem.umn.edu.

‡ Department of Chemistry.

§ Department of Biochemistry, Molecular Biology, and Biophysics.

[1] Abbreviations: PLN, phospholamban; SLN, sarcolipin; SERCA, sarco(endo)plasmic reticulum calcium ATPase; DOPC, dioleoyl-*sn*-glycero-3-phosphocholine; DOPE, dioleoyl-*sn*-glycero-3-phosphoethanolamine; CPMG, Carr−Purcell−Meiboom−Gill; wt-PLN, wild-type PLN; DC, dipolar coupling; CSA, chemical shift anisotropy.

10.1021/bi701668v CCC: $40.75
Published on Web 12/15/2007

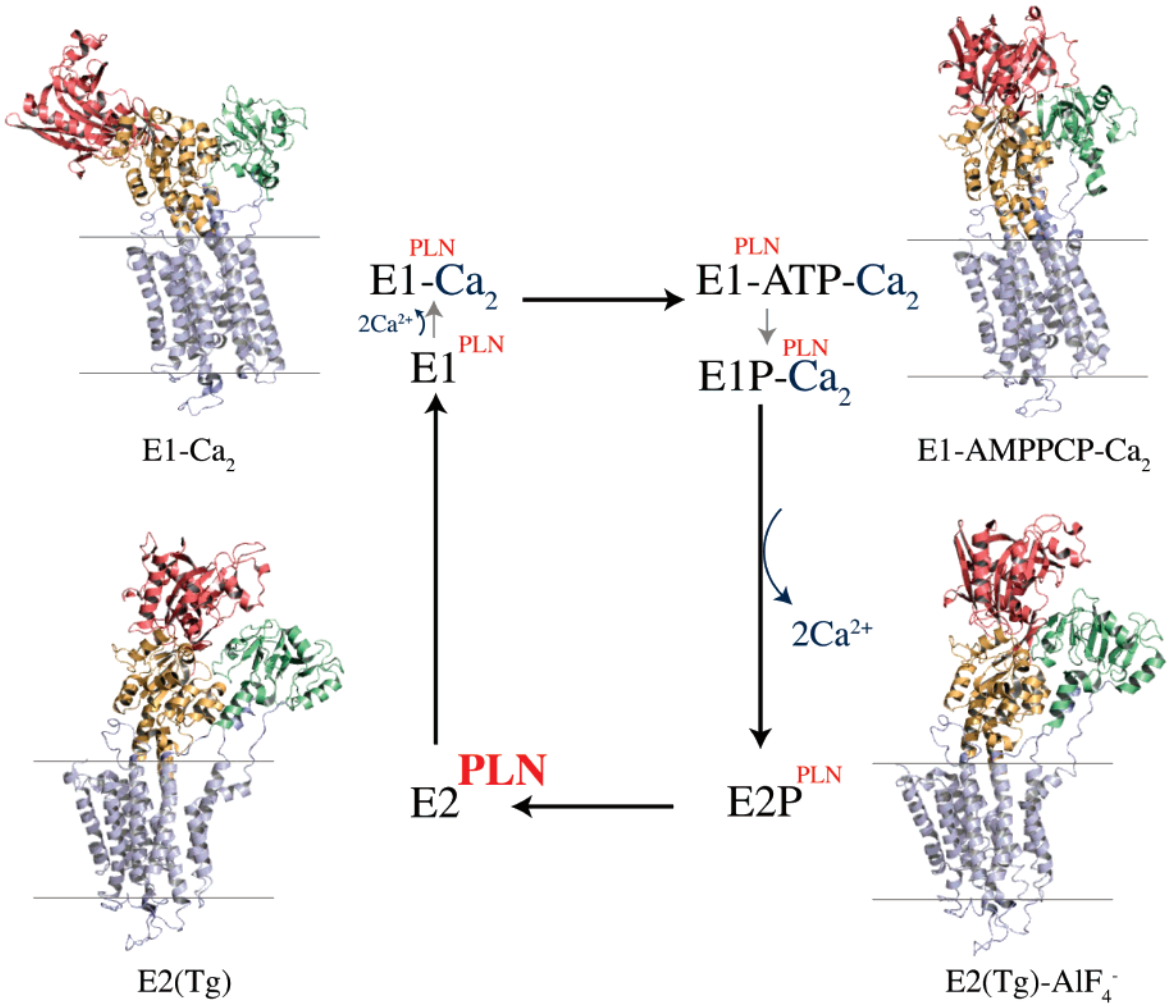

FIGURE 1: Proposed enzymatic cycle mimicking the four major conformational states of SERCA: E2 (1IWO) (*15*), E1-Ca_2 (1SU4) (*14*), E1-ATP-Ca_2 (1VFP) (*16*), and E2P (1XP5) (*18*). PLN and SLN are believed to inhibit the E2 conformation as indicated within the model.

the SERCA−PLN complex is a low-resolution cryoelectron microscopy image (8−10 Å) obtained by Stokes and co-workers (*20*). Hampering the formation of large, highly diffracting SERCA−PLN and SERCA−SLN cocrystals is the dynamic interplay between the proteins and lipids. For this reason, MacLennan and co-workers have used a plethora of biological data (mutagenesis studies, coimmunoprecipitation assays, and cross-linking experiments) in concert with molecular dynamics simulations to model SERCA−PLN (*21*), SERCA−SLN (*22*), and SERCA−PLN−SLN complexes (*22*) (Figure 2). Hutter et al. (*23*) have also modeled the solution structure of C41F PLN determined in a chloroform/methanol mixture with the E2 form of SERCA using molecular mechanics. While these models shed light on the interaction between SERCA and PLN and SLN, there are inconsistencies concerning the topology and structure of PLN and SLN within the complexes.

This review reports on our recent progress involving the structure determination of PLN and SLN and toward elucidation of the interaction with SERCA using solution and solid-state NMR. While many contributions to the structural analysis of PLN and SLN from other laboratories are cited and related to our work, this review is not intended to be an exhaustive overview of the large amount of structural and biological information about PLN and SLN within the literature.

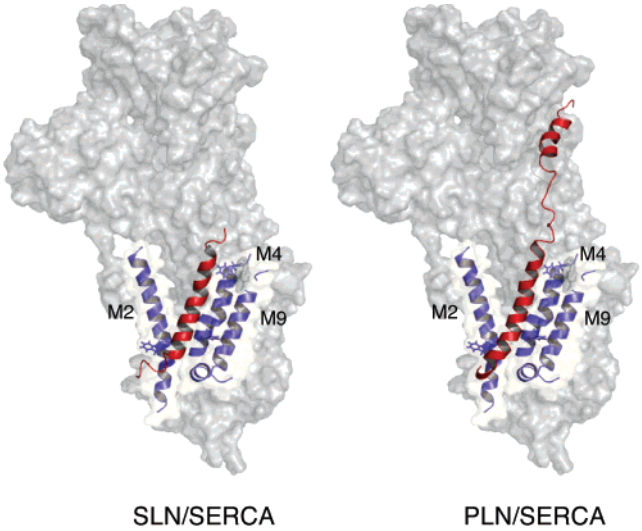

FIGURE 2: Molecular modeling of SERCA−SLN (*22*) and SERCA−PLN (*21*) complexes. Coordinates of complexes generously provided by D. H. Maclennan and C. Toyoshima.

Choice of Membrane Mimicking Environments for Spectroscopic Studies

For both solution and solid-state NMR, we use two major criteria for sample preparation: (1) functionality of proteins under NMR conditions and (2) the ability to acquire high-

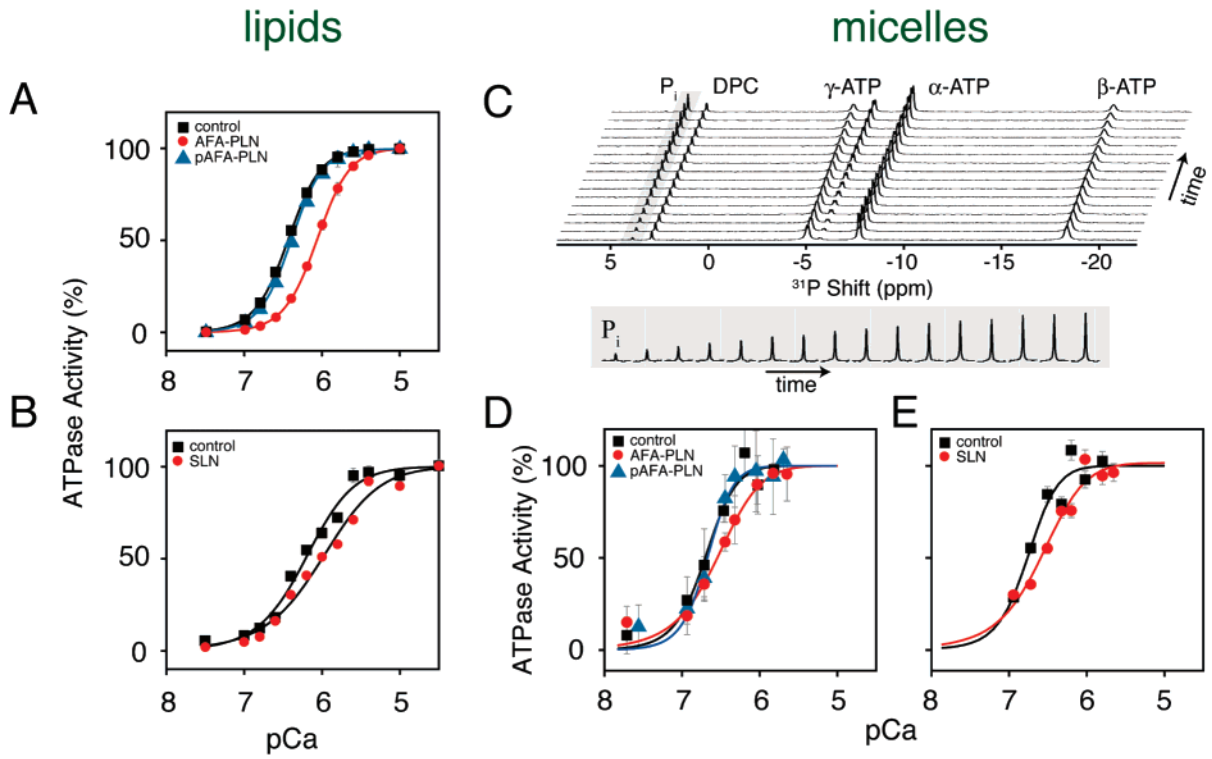

FIGURE 3: Activity assays of SERCA in the presence and absence of PLN and SLN in 4/1 DOPC/DOPE lipid bilayers (A and B) and DPC detergent micelles (D and E). SERCA activity in lipid bilayers was measured via the coupled enzyme assay and is reproduced with permission from ref *24*. Copyright 2003 Elsevier. The activity assays in DPC micelles were conducted using ^{31}P NMR spectroscopy (C) as previously reported (*26*). Reproduced with permission from refs *25* and *26*. Copyright 2006 Elsevier.

quality NMR spectra. Being membrane-embedded proteins, SLN and PLN need lipid environments to elicit their biological function. After scanning several different conditions, we chose dodecylphosphocholine (DPC) detergent micelles for solution NMR studies and a 4/1 mixture of dioleoyl-*sn*-glycero-3-phosphocholine and dioleoyl-*sn*-glycero-3-phosphoethanolamine (DOPC/DOPE) lipids for solid-state NMR studies. Panels A and B of Figure 3 show the calcium dependence of SERCA activity in the presence and absence of PLN (or SLN) under these conditions. The hydrolysis of ATP by SERCA in DPC micelles is followed directly using ^{31}P NMR spectroscopy and indirectly in lipids using the coupled enzyme assay (*24*−*26*). An example of the kinetics from the ^{31}P spectroscopic assay is shown in Figure 3C. The kinetics of ATP hydrolysis was determined by following the formation (build-up) of inorganic phosphate (Figure 3C). In both lipid bilayers and detergent micelles, SERCA samples are fully functional.

PLN Structure and Dynamics in DPC Micelles

In the SR, PLN is thought to exist as an inactive pentamer (storage form), which depolymerizes into functional monomers prior to interaction with SERCA (Figure 2) (*27*, *28*). Accordingly, we have focused our attention on a fully functional monomer of PLN (AFA-PLN) obtained by mutating the three cysteine residues (Cys-36, -41, and -46) of the transmembrane domain to Ala, Phe, and Ala, respectively. Using NOE restraints in structural calculations, we have determined that PLN adopts an L-shaped conformation in DPC micelles comprised of three distinct structural domains: cytoplasmic domain Ia helix (residue 1 to 16), loop (residue 17 to 22), and transmembrane domain helix (residue 23 to 52) (Figure 4A) (*29*). From simulated annealing calculations, we obtained a structural ensemble with very good convergence for each single structural domain (see ref *29*), but with the PLN conformers displaying an interhelical angle (angle between cytoplasmic and transmembrane domains) of 80 ± 22° (Figure 4A). Indeed, the limited number of NOEs detected in the loop did not allow us to restrain the two helical domains and obtain an ensemble of structures with a low RMSD over the entire protein backbone. Because of the lack of convergence on the orientation of helical domain Ia with respect to the surface of the micelle, we used Mn^{2+} and 5′- and 16′-doxyl stearic acids as paramagnetic probes of the topological arrangement of PLN in the micelle (*29*). Our results show that Mn^{2+} ions cause a reduction in the resonance intensities of residues located at both termini, the loop, and Ser-16 and Thr-17, showing that both phosphorylation sites are solvent-exposed. Both 5′- and 16′-doxyl stearic acids caused a reduction in the resonance intensities of residues located in the micellar region. 16′-Doxyl stearic acid affected residues in the core of the micelle (residues 35−45), as well as Leu-7, located in the middle of domain Ia, a residue that is likely buried in the hydrophobic region of the micelle. At higher 16′-doxyl stearic acid/PLN ratios, domain Ia is also considerably affected by the paramagnetic center, with Ala-11 displaying a reduced resonance intensity.

Our structural ensemble of the PLN monomer is in qualitative agreement with studies carried out in organic solvents (*30*, *31*), where the authors found an overall L-shaped structure of PLN with the intervening loop in either a short flexible turn or a type III β-turn conformation. However, we found an orientation of the cytoplasmic helix, which is in better agreement with the amphipathicity of the PLN

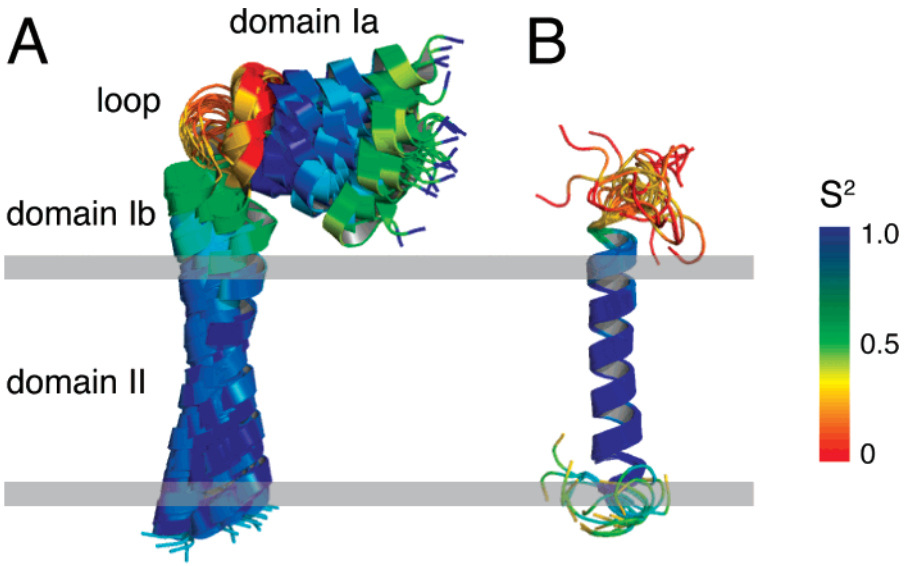

FIGURE 4: (A) Backbone overlay of PLN from PDB entry 1N7L (*29*). (B) Backbone overlay of SLN as reported by Buffy et al. (*25*). The color coding on the structures corresponds to the order parameters (S^2) as previously determined (*32*, *33*).

sequence (*29*). The most relevant PLN conformations in PDB entry 1N7L are those in which the hydrophobic side chains in domain Ia (Val-4, Leu-7, Ala-11, and Ala-15) are oriented toward the interior of the micelle and the hydrophilic residues point toward the bulk solvent, rendering the two phosphorylation sites exposed for interaction with protein kinases.

While our NMR structural studies identified three structural domains, nuclear spin relaxation measurements and solvent accessibility experiments carried out on uniformly ^{15}N-labeled PLN (*32*, *33*) further subdivided the helical segment from residue 23 to 52 into two domains: domain Ib (residues 23−30), which is more dynamic and constituted by hydrophilic residues, and domain II (31−52), more hydrophobic and motionally restricted. Therefore, we can divide PLN into four dynamic regions, which are characterized by different order parameters (see Figure 4A). Carr−Purcell−Meiboom−Gill (CPMG)-based relaxation measurements also indicated the presence of slow dynamics (microsecond to millisecond motion) in domain Ia, the loop, and domain Ib (*32*, *33*). While the slow dynamics of domain Ia and the loop were predicted on the basis of the H−D exchange factors, the flexibility of residues within domain Ib was unexpected. The plasticity of this region supports biological evidence for the great importance of domain Ib and the molding necessary to fit into the binding groove of SERCA (*21*, *34*).

Recently, a structure of wild-type PLN (wt-PLN) was reported showing the pentamer to be in a bellflower arrangement, where the cytoplasmic domain helix of each monomer makes an ~20° angle with respect to the bilayer normal (*35*), substantially different from the topology we reported for monomeric AFA-PLN (*29*). Our recent studies using solution NMR and EPR in DPC detergent micelles also point toward a dominating L-shaped conformation (or pinwheel model) for the pentamer (*36*). We also looked at the topology of pentameric wt-PLN in lipid bilayers using solid-state NMR, finding unambiguous evidence for the pinwheel model (see below).

SLN Structure and Dynamics in Micelles

The initial structure of SLN was determined in sodium dodecyl sulfate (SDS) micelles using a synthetic polypeptide (*37*). Under these experimental conditions, SLN has an α-helical conformation from residue Phe-9 to Arg-27 with RMSDs of 0.65 and 1.66 Å for backbone and side chain atoms, respectively. Both the N-terminus (M1−L8) and the C-terminus (S28−Y31) were found to be unstructured. Subsequently, we expressed uniformly ^{15}N-labeled recombinant SLN in *Escherichia coli*, which enabled the use of higher-resolution ^{1}H−^{15}N NMR experiments to reduce several ambiguities due to resonance overlap. With recombinant SLN, we determined the structure in DPC micelles, conditions that ensured the activity of SERCA, and found it to remain a single transmembrane helix with approximately five unstructured residues at either terminus (*25*). The superposition of the C_α, N_H, and C′ backbone atoms from residue Arg-6 to Arg-27 gave an RMSD of 0.4 ± 0.2 Å with an RMSD of 1.7 ± 0.3 Å for side chain atoms.

In addition to structure determination, we also measured spin relaxation rates and found that the backbone dynamics, similar to that of PLN, is more complex than the structure. Relaxation measurements reveal four dynamic domains: a short unstructured N terminus (residues 1−6), a short dynamic helix (residues 7−14), a more rigid helix (residues 15−26), and an unstructured C-terminus (residues 27−31) (*25*). H−D exchange factors also support the existence of four dynamic domains (*25*). The similarity of SLN structure and dynamics with those of PLN domains Ib and II shows that sequence conservation is reflected in the conservation of both structure and dynamics (Figure 4B).

PLN and SLN Topologies and Dynamics in Lipid Bilayers

Solid-state NMR in lipid bilayers has emerged as a complement to solution NMR studies in detergent micelles for elucidating structure, dynamics, and interactions between membrane proteins (*38*, *39*). For our first solid-state NMR studies, we synthesized AFA-PLN labeled with ^{15}N at Ala-11, Ala-15, and Ala-36 and measured the ^{15}N chemical shift anisotropy in 4/1 DOPC/DOPE mechanically oriented lipid bilayers on glass plate supports (*40*). Using these solid-state NMR measurements in concert with rigid body molecular mechanics, we found that domains Ib and II are oriented approximately perpendicular to the plane of the

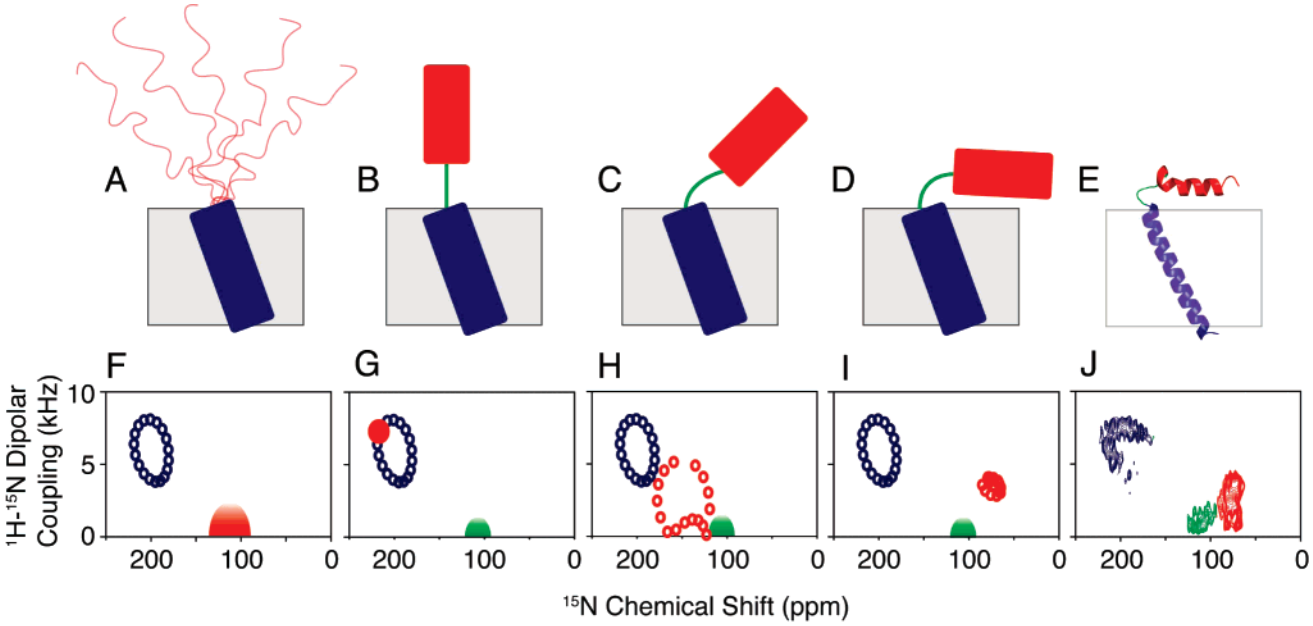

FIGURE 5: Structural models (A−D) proposed for PLN in lipid bilayers with PISEMA simulations (F−I). The ensemble of conformers reported by our laboratory (PDB entry 1N7L) is shown in panel E (*29*). The colors are coded with the regions of the protein: red for cytoplasmic, blue for transmembrane, and green for loop regions. The L-shaped topology (D and E) agrees best with the experimental PISEMA (J). Reproduced with permission from ref *42*. Copyright 2006 American Chemical Society.

bilayer with the interhelical (i.e., interdomain) angle ranging between 60 and 100°, ruling out the possibility of a continuous α-helix and also suggesting that the cytoplasmic domain of PLN interacts with the membrane surface.

Similar solid-state NMR measurements on SLN oriented in mechanically aligned DOPC/DOPE bilayers revealed the approximate parallel orientation of the SLN helix with respect to the membrane bilayer normal (*37*). Since the limited number of labeled sites did not allow us to give quantitative topological angles for SLN and PLN within the bilayer, we then proceeded to use two-dimensional (2D) ^{1}H−^{15}N PISEMA (polarization inversion spin exchange at the magic angle) experiments (*41*). This separated-local-field experiment correlates the ^{15}N chemical shift anisotropy (CSA) with the ^{1}H−^{15}N dipolar coupling (DC). Since the values of both CSA and DC depend on the orientation of the peptide plane with respect to the direction of the magnetic field, the assignment of the amide resonances allows for the determination of the structure and topology in aligned lipid bilayers.

We determined that in mixed 4/1 DOPC/DOPE lipid bilayers, AFA-PLN has an overall L-shaped conformation where the helix comprising domains Ib and II makes a tilt angle of ∼21° with respect to the bilayer normal (*42*). As expected from the one-dimensional (1D) solid-state NMR studies on synthetically ^{15}N-labeled AFA-PLN (*37*), PISEMA NMR spectroscopy clearly shows that domain Ia interacts with the membrane surface, making an angle of ∼90° with respect to the bilayer normal (*42*). A current model of the PLN monomer is reported in Figure 5E.

In addition to the structural and topological information obtained from oriented alignments, tilting the aligned samples to different angles with respect to the direction of the static field makes it possible to investigate the rotational dynamics of the protein within the bilayer (*43*−*45*). Tilting the AFA-PLN sample by 90° revealed that domains Ib and II undergo fast long-axial rotational diffusion about the bilayer normal with the cytoplasmic domain undergoing this motion and other complex dynamics, scaling both the values of CSA and DC (*42*). The dynamics detected in both our solution and solid-state NMR experiments may explain variability within the literature regarding the topology of the cytoplasmic domain of PLN. For example, a magic-angle-spinning (MAS) solid-state NMR study carried out by Baldus and co-workers found that while cross-polarization (CP)-based pulse sequences were adequate for detection of the transmembrane domain of AFA-PLN, showing the existence of a well-defined helix, the cytoplasmic domain residues were too dynamic to be detected (*46*). Instead, *J* coupling coherence transfers, similar to those in solution NMR experiments, were used to detect the dynamic cytoplasmic domain, leading to the conclusion that the cytoplasmic domain was completely unstructured. While this study represents an advancement in MAS methodology, the structure most likely represents a minor conformational state and is inconsistent with a wealth of data, including those from our laboratory, which consistently show a predominant helical cytoplasmic domain with an overall L-shaped monomeric structure in lipid bilayers and detergent micelles.

A close inspection of PISEMA spectra from selectively labeled samples reveals the presence of two peak populations that exemplify two slightly different topologies for AFA-PLN domains Ib and II (*42*). The two topologies have the same tilt angle (θ) for domains Ib and II with respect to the membrane normal, but slightly different rotational angles around the helix axis (ρ). Multiple populations of PLN have also been observed by the Lorigan and Middleton groups using MAS NMR experiments in lipid vesicles (*47*, *48*). The detection of multiple conformers underscores the plasticity of PLN and might be an important recognition mechanism for SERCA, protein kinase A, Ca^{2+}/calmodulin-dependent protein kinase, and protein phosphatase 1, previously shown to be necessary for physiological processes (*34*).

As with those of AFA-PLN, the PISEMA spectra of SLN obtained on uniformly ^{15}N-labeled and selectively labeled

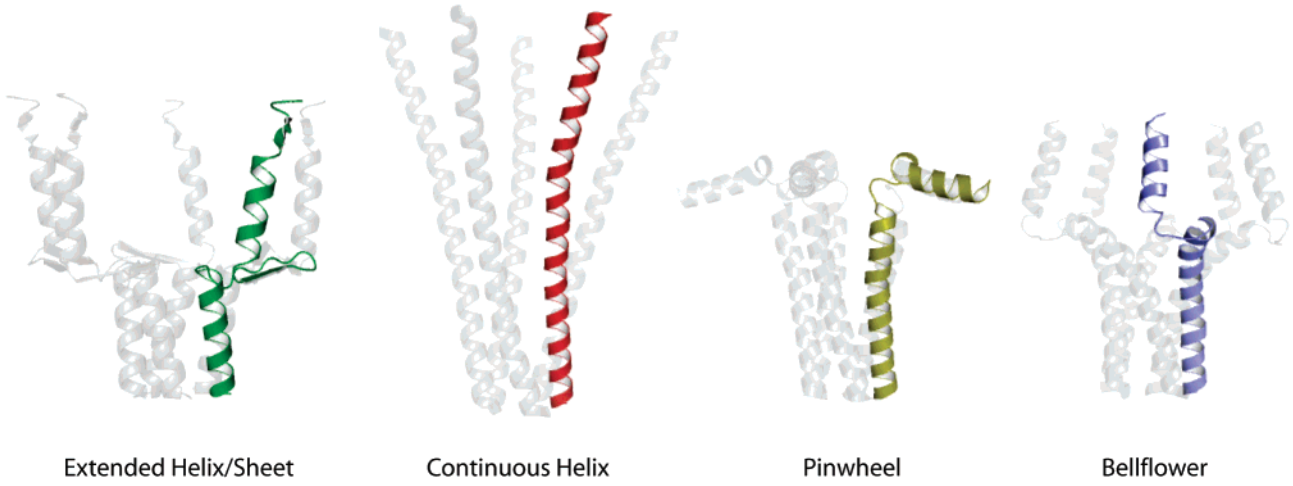

FIGURE 6: Structural models of wt-PLN. The pinwheel (1XNU) and bellflower (1ZLL) pentamer models were taken directly from PDB coordinates. Reproduced with permission from ref *36*. Copyright 2007 National Academy of Sciences of the United States of America.

[^{15}N-Leu], [^{15}N-Ile], and [^{15}N-Val] samples also revealed the existence of two distinct topologies (*49*). Both the major and the minor populations of the resonances corresponding to domains Ib and II are oriented ~23° with respect to the lipid bilayer normal but vary in the rotation angle about the helical axis by ~5° (in remarkable agreement with AFA-PLN). The primary sequence homology between SLN and PLN results in nearly identical structural and dynamic properties of these two regulatory proteins.

Pentameric wt-PLN Topology in Lipid Bilayers

More recently, our group has embarked on the validation of the pentameric structure of wt-PLN in lipid bilayers and detergent micelles (*36*). While monomeric PLN has previously been shown to bind and inhibit SERCA, recently it was hypothesized that the pentamer could also bind and inhibit SERCA (*50*). While there is broad consensus regarding the secondary structure of pentameric wt-PLN, there is disagreement in the literature about the orientation of the cytoplasmic helix. In particular, there are four proposed models for pentameric wt-PLN (Figure 6). The first model (extended helix/sheet) shows wt-PLN to be comprised of two α-helices connected by an antiparallel β-sheet (residues 22−32), where the cytoplasmic domain is oriented 50−60° relative to the bilayer normal (*51*). The second model depicts wt-PLN as a continuous α-helix with a tilt angle of 28 ± 6° with respect to the bilayer normal (*52*, *53*). The third model (pinwheel) shows that the most stable pentamer has a pinwheel geometry in which the cytoplasmic domain helices are oriented ~90° with respect to the membrane bilayer normal (*54*). The fourth and most recent model (bellflower) shows the structure of the pentamer to be in a bellflower assembly with the cytoplasmic domain helices oriented ~20° with respect to the bilayer normal (*35*).

To study the topology of pentameric wt-PLN, we reconstituted the protein in mechanically aligned 4/1 DOPC/DOPE lipid bilayers and analyzed the protein's architecture using ^{1}H−^{15}N PISEMA spectroscopy. As with the AFA-PLN monomer (*42*), we found that the wt-PLN PISEMA spectrum is composed of three different populations of resonances (see the 1D spectrum in Figure 7A) corresponding to domains Ib and II (with the resonances located between 170 and 220 ppm), an in-plane cytoplasmic domain (with resonances located between 50 and 100 ppm), and a more flexible region (loop and termini) with resonances clustered around ~110 ppm (isotropic portion of the spectrum). Since our 1D spectrum shows three distinct regions, indicating three unique wt-PLN domain alignments with respect to the membrane bilayer normal, this eliminates the possibility of the continuous helix model.

To distinguish among the other models depicted in Figure 6, we performed PISEMA experiments using selectively labeled [^{15}N-Ala], [^{15}N-Thr], [^{15}N-Leu], [^{15}N-Ile], [^{15}N-Cys], and [^{15}N-Asn] wt-PLN samples. Our experimental PISEMA spectra, reported as an overlay in Figure 7, show a remarkable similarity with the AFA-PLN monomer. In fact, simulations for domain Ia resonances (Leu-7, Thr-8, Ala-11, Ile-12, Ala-15, Thr-17, and Ile-18) correspond to a helix with a tilt angle of ~90° with respect to the bilayer normal (Figure 7E) (*36*).

Figure 8 shows PISEMA spectra simulated from the pinwheel and bellflower PDB coordinates for those selectively labeled sites shown in Figure 7. If the pentamer topology corresponded to the pinwheel model, the cytoplasmic domain residues would resonate in the upfield region of the spectrum (50−100 ppm) (Figure 8A). On the other hand, if the architecture of wt-PLN were consistent with the bellflower model, domain Ia resonances in the PISEMA pattern would occupy the downfield portion of the spectrum (170−220 ppm), as represented in Figure 8B. If the experimental domain Ia spectra are compared, it is clear that in lipid bilayers the cytoplasmic domain Ia is oriented perpendicular with the bilayer normal forming an overall pinwheel geometry.

Structural fitting with an ideal helix in Figure 7D revealed that the helix corresponding to domains Ib and II of pentameric wt-PLN has a tilt angle (θ) of ~15° with respect to the bilayer normal (*36*). Monomeric AFA-PLN has a tilt angle of ~21° (*42*), which requires pentamer formation to tilt by ~6° to accommodate the leucine/isoleucine zipper holding the pentamer together (*55*, *56*).

Allosteric Activation Model

The functionality of SERCA under NMR conditions and the quality of AFA-PLN spectra upon addition of SERCA

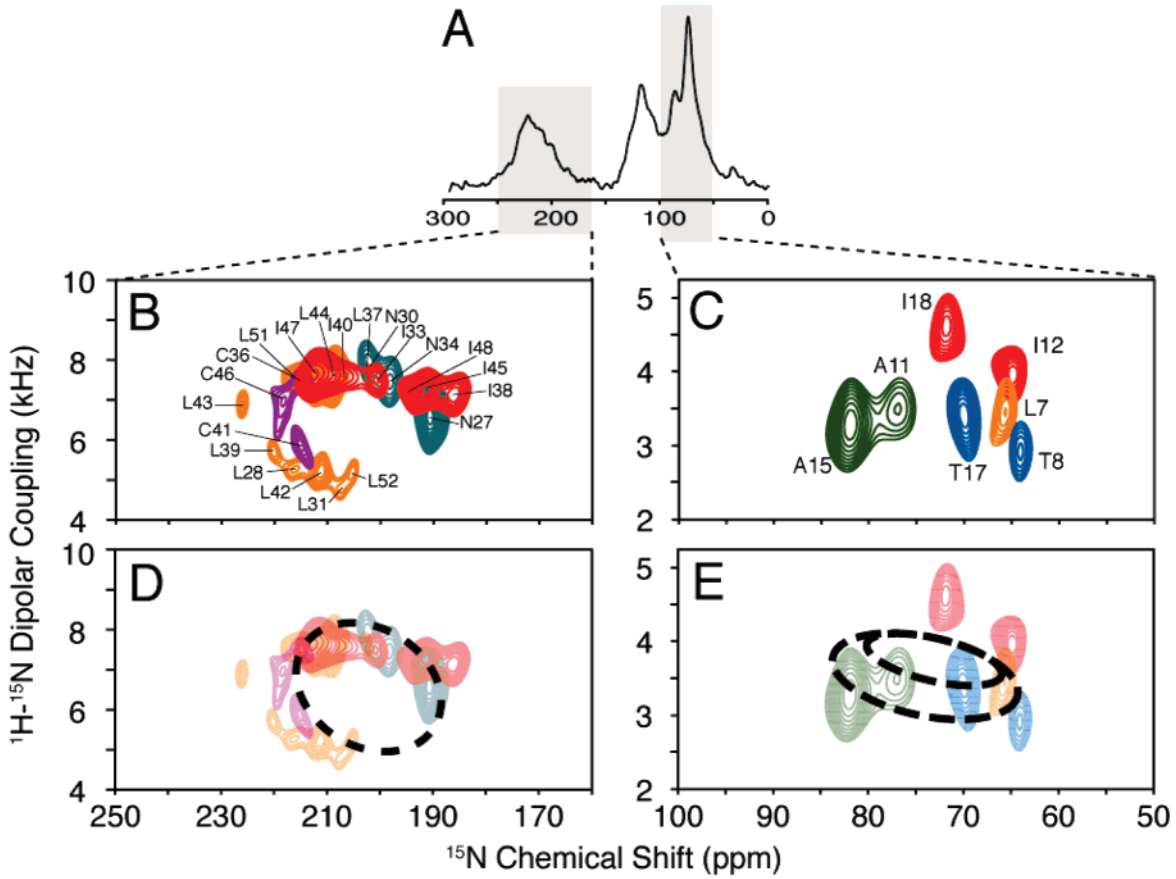

FIGURE 7: PISEMA spectra of the PLN pentamer in lipid bilayers. (A) 1D cross-polarization spectrum of [U-^{15}N]wt-PLN in DOPC/DOPE oriented lipid bilayers. (B and C) Selectively labeled wt-PLN PISEMA spectra for the transmembrane and cytoplasmic helices, respectively. The residues are color coded with the PISEMA spectra: green for [^{15}N-Ala], purple for [^{15}N-Cys], orange for [^{15}N-Leu], red for [^{15}N-Ile], gray for [^{15}N-Asn], and blue for [^{15}N-Thr]. (D and E) Simulated PISA wheels for both transmembrane ($\theta = 15°$) and cytoplasmic ($\theta = 92°$) domains. Reproduced with permission from ref *36*. Copyright 2007 National Academy of Sciences of the United States of America.

enabled the unprecedented atomic mapping of the interactions between these two integral membrane proteins in detergent micelles (*57*). In its free form, AFA-PLN exists in a dynamic equilibrium between two conformations, T and R states, where the T state or L-shaped conformation is thermodynamically stable and the R state or extended form is identified with a more dynamic cytoplasmic domain (Figure 9) (*57*, *58*). These two states are readily detected using EPR spectroscopy in both micelles and lipid bilayers (*57*, *58*), but due to the time scale of the exchange, NMR can only imply the existence of these forms from relaxation dispersion measurements (i.e., conformational interconversion). However, upon addition of SERCA to AFA-PLN, chemical shift perturbation analyses reveal the appearance of a second population of peaks within domain Ia, the loop, and domain Ib, indicating a conformational switch of AFA-PLN from the T state to the R state, exemplifying an allosteric activation mechanism (*57*).

Resonances from the hydrophobic portion of the transmembrane region (domain II) also show chemical exchange to the R state (*26*). A difference plot of the ^1H_N chemical shift before and after addition of SERCA for residues within domain II (residues 31−52) shows a symmetric bimodal behavior where the C-terminal part of domain II shifted upfield and the residues near the N-terminal part downfield (*26*). Since upfield and downfield shifts have been correlated to the strength of hydrogen bonds (*59*), one possible explanation for the data is that the C-terminal end of the transmembrane domain (residues 46−52) unwinds upon binding SERCA. This hypothesis was first proposed by MacLennan and co-workers (*21*), who indicated an overall change in the secondary structure of the domain II, with residues 49−52 unwinding upon interaction with SERCA, a process that might facilitate binding.

These results are echoed in the binding of SLN to SERCA (*25*). Overall, SLN behaves like the domains Ib and II of AFA-PLN, with each dynamic domain mimicking the behavior of the corresponding domain in AFA-PLN. Upon addition of SERCA, the transmembrane domain is in fast exchange between two free forms (T and R states). As previously indicated, spin relaxation measurements divided the transmembrane domain of SLN into two regions we named domain Ib and domain II in analogy with AFA-PLN. The chemical shift changes of these two regions follow the bimodal behavior of the transmembrane domain of AFA-PLN, indicative of a similar mechanism involving an unwinding of the C-terminal residues and a stabilization of the residues in the N-terminal portion of the protein as a result of the interactions with SERCA (*25*). This supports the hypothesis that both SLN and PLN transmembrane domains bind SERCA in the same site and with an identical mechanism.

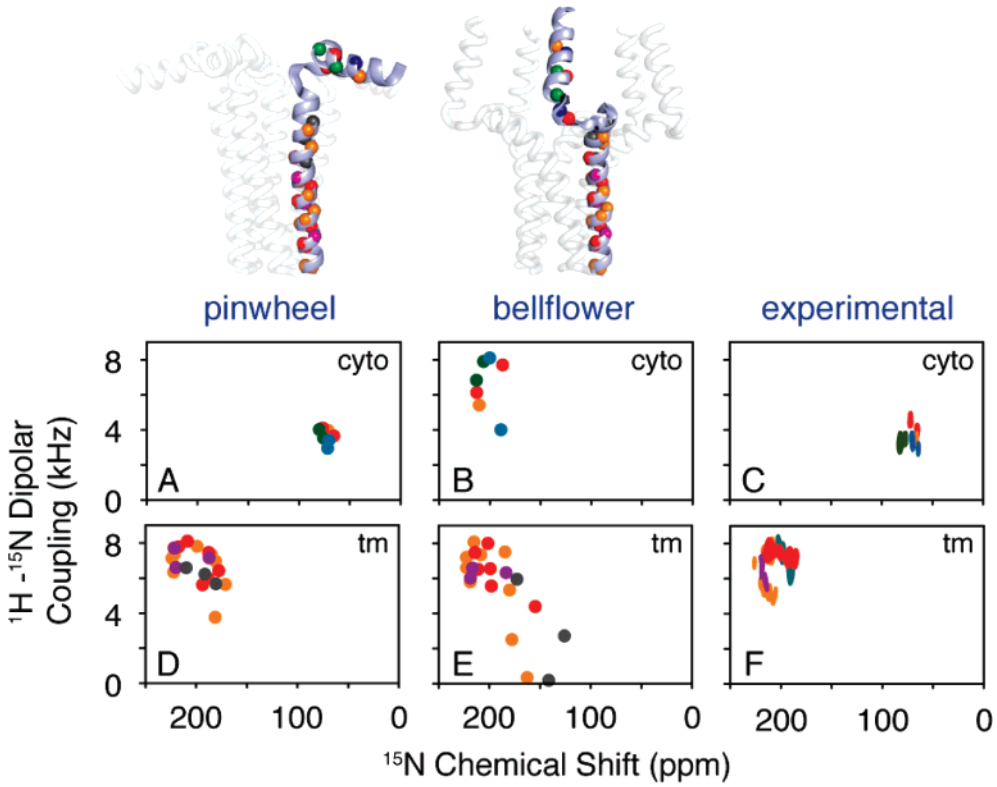

FIGURE 8: Simulated and experimental PISEMA spectra for the pinwheel and bellflower models. Unlike the pinwheel model, the bellflower model shows no high-field resonances. Experimental PISEMA spectra (C and F) show the remarkable agreement with the pinwheel model (A and D). Reproduced with permission from ref *36*. Copyright 2007 National Academy of Sciences of the United States of America.

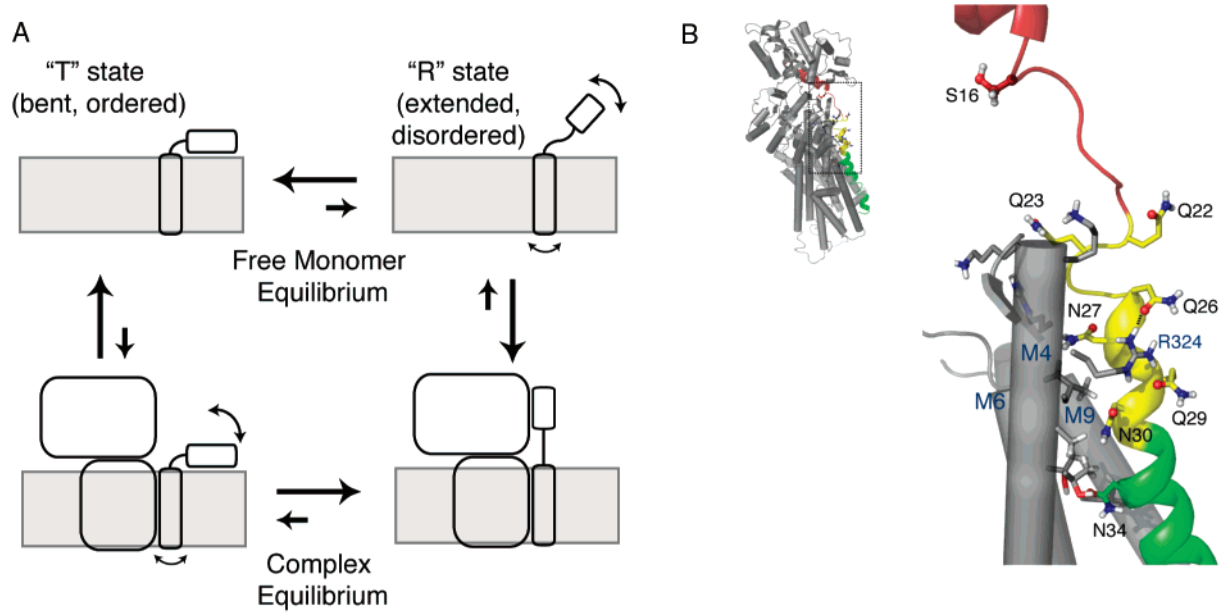

FIGURE 9: (A) Allosteric model of interaction of PLN with SERCA. The PLN monomer interconverts between the L-shaped form (T state) and the less stable (more dynamically disordered) extended form (R state). (B) PLN−SERCA model developed by Toyoshima et al. (*21*) highlighting the long-range allosteric control phosphorylation at Ser-16 has on domain Ib. Panel A reproduced with permission from ref *57*. Copyright 2005 National Academy of Sciences of the United States of America. Panel B reproduced with permisson from ref *26*. Copyright 2006 Elsevier.

Effects of PLN Phosphorylation on the Allosteric Mechanism

The inhibition of SERCA by PLN can be reversed by phosphorylation at Ser-16 by cAMP-dependent protein kinase A (*2*). We determined the structure of Ser-16-phosphorylated AFA-PLN (pS16-AFA-PLN) and found that residues 14−16, previously helical, became unwound upon phosphorylation, revealing an order-to-disorder transition (*33*). In addition, we found that there are pronounced changes in pS16-AFA-PLN backbone dynamics on both the picosecond to nanosecond and microsecond to millisecond time scales (*33*). Although small, some of the changes are propagated throughout the entire protein backbone, demonstrating that while the structural transitions following phosphorylation are

localized, the changes in backbone dynamics are radiated throughout the protein.

How can this order-to-disorder transition help in understanding the interaction with SERCA? To answer this question, we proceeded with the analysis of the chemical shift perturbation of pS16-AFA-PLN induced by SERCA (*26*). We found that the conformational equilibrium between the T and R states upon addition of SERCA is influenced by single phosphorylation at Ser-16; specifically, phosphorylation shifts the equilibrium toward the R state in a cooperative manner (*26*). Another considerable difference upon phosphorylation includes a change in both the surface and the dynamics of domain Ib. In particular, a remarkable change is observed for the side chain binding behavior. In constrast with unphosphorylated PLN, the Gln-26 resonance in the phosphorylated protein is unperturbed by SERCA with other smaller changes seen for side chain residues Asn-27, -30, and -34. A possible mechanism for explaining these results is the rotation or rearrangement of domain Ib upon phosphorylation that disrupts crucial intermolecular hydrogen bonds, resulting in relief of inhibition. On the basis of the molecular model of MacLennan and co-workers (*21*), we proposed that a crucial hydrogen bond between Arg-324 and Gln-26 may be broken between SERCA and PLN after phosphorylation at Ser-16 (*26*). These findings are in agreement with mutagenesis studies, showing that Q26A is a loss-of-function mutant (*60*). In addition, cross-linking studies show that an N27C mutation in pS16-AFA-PLN is no longer able to cross-link with SERCA (*21*). While there are changes in the binding interface for domain Ib, the overall binding of domain II to SERCA is not affected by phosphorylation. The dissociation constants (K_d) for domain II in both pS16-AFA-PLN and AFA-PLN are ~60 μM (*26*). This demonstrates that the major changes are in domain Ia, loop, and domain Ib, with domain II only marginally affected, supporting the hypothesis that phosphorylation at Ser-16 does not dissociate PLN from SERCA completely. We proposed domain Ib as a bridgehead region, which transmits the dynamics induced by phosphorylation at Ser-16 from domain Ia to domain Ib, thereby regulating the intramembrane protein−protein interaction (*26*). A schematic of the allosteric model for phosphorylation is reported in Figure 9.

Perspective

What can we learn from the analysis of the structure and dynamics of PLN? More importantly, how are structure and dynamics of PLN correlated to SERCA's function, and can we control the extent of inhibition of SERCA by manipulating PLN structural dynamics? These are questions we have begun to address in our recent publication, showing that indeed it is possible to control SERCA's activity by tuning PLN structural dynamics (*62*). We will continue to tackle these questions in the upcoming years.

Given the plethora of biochemical and molecular biology data currently available, it is a very exciting moment for structural biologists involved in research on PLN and SLN and their interactions with SERCA. While our studies to date have focused on monitoring the effects of PLN induced by SERCA, our future challenge involves detecting SERCA changes from PLN within the entire enzymatic cycle. Another important challenge is to study the SERCA−PLN complex in the complex network of interactions involving protein kinase A and protein phosphatase 1. While solution NMR will help identify some important pieces of this complex puzzle, solid-state NMR will be the method of choice for the elucidation of the structural dynamics and interactions in these large complexes.

ACKNOWLEDGMENT

We are grateful to the former members of the Veglia Laboratory (Alessandro Mascioni, Bethany Buck-Koehntop, Jamillah Zamoon, and Emily Metcalfe) and for the productive collaboration with the laboratory of David Thomas.

REFERENCES

1. Fujii, J., Ueno, A., Kitano, K., Tanaka, S., Kadoma, M., and Tada, M. (1987) Complete Complementary DNA-Derived Amino Acid Sequence of Canine Cardiac Phospholamban, *J. Clin. Invest. 79*, 301−304.
2. Wegener, A. D., Simmerman, H. K., Lindemann, J. P., and Jones, L. R. (1989) Phospholamban Phosphorylation in Intact Ventricles. Phosphorylation of Serine 16 and Threonine 17 in Response to β-Adrenergic Stimulation, *J. Biol. Chem. 264*, 11468−11474.
3. Mundina-Weilenmann, C., Vittone, L., Ortale, M., de Cingolani, G. C., and Mattiazzi, A. (1996) Immunodetection of Phosphorylation Sites Gives New Insights into the Mechanisms Underlying Phospholamban Phosphorylation in the Intact Heart, *J. Biol. Chem. 271*, 33561−33567.
4. Chu, G., Lester, J. W., Young, K. B., Luo, W., Zhai, J., and Kranias, E. G. (2000) A Single Site (Ser16) Phosphorylation in Phospholamban is Sufficient in Mediating its Maximal Cardiac Responses to β-Agonists, *J. Biol. Chem. 275*, 38938−38943.
5. Wawrzynow, A., Theibert, J. L., Murphy, C., Jona, I., Martonosi, A., and Collins, J. H. (1992) Sarcolipin, the "Proteolipid" of Skeletal Muscle Sarcoplasmic Reticulum, is a Unique, Amphipathic, 31-Residue Peptide, *Arch. Biochem. Biophys. 298*, 620−623.
6. Odermatt, A., Taschner, P. E., Scherer, S. W., Beatty, B., Khanna, V. K., Cornblath, D. R., Chaudhry, V., Yee, W. C., Schrank, B., Karpati, G., Breuning, M. H., Knoers, N., and MacLennan, D. H. (1997) Characterization of the Gene Encoding Human Sarcolipin (SLN), a Proteolipid Associated with SERCA1: Absence of Structural Mutations in Five Patients with Brody Disease, *Genomics 45*, 541−553.
7. Gayan-Ramirez, G., Vanzeir, L., Wuytack, F., and Decramer, M. (2000) Corticosteroids Decrease mRNA Levels of SERCA Pumps, Whereas they Increase Sarcolipin mRNA in the Rat Diaphragm, *J. Physiol. 524* (Part 2), 387−397.
8. Minamisawa, S., Wang, Y., Chen, J., Ishikawa, Y., Chien, K. R., and Matsuoka, R. (2003) Atrial Chamber-Specific Expression of Sarcolipin is Regulated during Development and Hypertrophic Remodeling, *J. Biol. Chem. 278*, 9570−9575.
9. Babu, G. J., Bhupathy, P., Carnes, C. A., Billman, G. E., and Periasamy, M. (2007) Differential Expression of Sarcolipin Protein during Muscle Development and Cardiac Pathophysiology, *J. Mol. Cell. Cardiol. 43*, 215−222.
10. Maclennan, D. H., Yip, C. C., Iles, and Seeman, P. (1972) Isolation of Sarcoplasmic Reticulum Proteins, *Cold Spring Harbor Symp. Quant. Biol. 37*, 469−478.
11. Odermatt, A., Becker, S., Khanna, V. K., Kurzydlowski, K., Leisner, E., Pette, D., and MacLennan, D. H. (1998) Sarcolipin Regulates the Activity of SERCA1, the Fast-Twitch Skeletal Muscle Sarcoplasmic Reticulum Ca^{2+}-ATPase, *J. Biol. Chem. 273*, 12360−12369.
12. Uemura, N., Ohkusa, T., Hamano, K., Nakagome, M., Hori, H., Shimizu, M., Matsuzaki, M., Mochizuki, S., Minamisawa, S., and Ishikawa, Y. (2004) Down-Regulation of Sarcolipin mRNA Expression in Chronic Atrial Fibrillation, *Eur. J. Clin. Invest. 34*, 723−730.
13. Gramolini, A. O., Trivieri, M. G., Oudit, G. Y., Kislinger, T., Li, W., Patel, M. M., Emili, A., Kranias, E. G., Backx, P. H., and Maclennan, D. H. (2006) Cardiac-Specific Overexpression of Sarcolipin in Phospholamban Null Mice Impairs Myocyte Function that is Restored by Phosphorylation, *Proc. Natl. Acad. Sci. U.S.A. 103*, 2446−2451.

14. Toyoshima, C., Nakasako, M., Nomura, H., and Ogawa, H. (2000) Crystal Structure of the Calcium Pump of Sarcoplasmic Reticulum at 2.6 Å Resolution, *Nature 405*, 647−655.
15. Toyoshima, C., and Nomura, H. (2002) Structural Changes in the Calcium Pump Accompanying the Dissociation of Calcium, *Nature 418*, 605−611.
16. Toyoshima, C., and Mizutani, T. (2004) Crystal Structure of the Calcium Pump with a Bound ATP Analogue, *Nature 430*, 529−535.
17. Toyoshima, C., Nomura, H., and Tsuda, T. (2004) Lumenal Gating Mechanism Revealed in Calcium Pump Crystal Structures with Phosphate Analogues, *Nature 432*, 361−368.
18. Olesen, C., Sorensen, T. L., Nielsen, R. C., Moller, J. V., and Nissen, P. (2004) Dephosphorylation of the Calcium Pump Coupled to Counterion Occlusion, *Science 306*, 2251−2255.
19. Sorensen, T. L., Moller, J. V., and Nissen, P. (2004) Phosphoryl Transfer and Calcium Ion Occlusion in the Calcium Pump, *Science 304*, 1672−1675.
20. Young, H. S., Jones, L. R., and Stokes, D. L. (2001) Locating Phospholamban in Co-Crystals with Ca^{2+}-ATPase by Cryoelectron Microscopy, *Biophys. J. 81*, 884−894.
21. Toyoshima, C., Asahi, M., Sugita, Y., Khanna, R., Tsuda, T., and MacLennan, D. H. (2003) Modeling of the Inhibitory Interaction of Phospholamban with the Ca^{2+} ATPase, *Proc. Natl. Acad. Sci. U.S.A. 100*, 467−472.
22. Asahi, M., Sugita, Y., Kurzydlowski, K., De Leon, S., Tada, M., Toyoshima, C., and MacLennan, D. H. (2003) Sarcolipin Regulates Sarco(Endo)Plasmic Reticulum Ca^{2+}-ATPase (SERCA) by Binding to Transmembrane Helices Alone or in Association with Phospholamban, *Proc. Natl. Acad. Sci. U.S.A. 100*, 5040−5045.
23. Hutter, M. C., Krebs, J., Meiler, J., Griesinger, C., Carafoli, E., and Helms, V. (2002) A Structural Model of the Complex Formed by Phospholamban and the Calcium Pump of Sarcoplasmic Reticulum obtained by Molecular Mechanics, *ChemBioChem 3*, 1200−1208.
24. Buck, B., Zamoon, J., Kirby, T. L., DeSilva, T. M., Karim, C., Thomas, D., and Veglia, G. (2003) Overexpression, Purification, and Characterization of Recombinant Ca-ATPase Regulators for High-Resolution Solution and Solid-State NMR Studies, *Protein Expression Purif. 30*, 253−261.
25. Buffy, J. J., Buck-Koehntop, B. A., Porcelli, F., Traaseth, N. J., Thomas, D. D., and Veglia, G. (2006) Defining the Intramembrane Binding Mechanism of Sarcolipin to Calcium ATPase using Solution NMR Spectroscopy, *J. Mol. Biol. 358*, 420−429.
26. Traaseth, N. J., Thomas, D. D., and Veglia, G. (2006) Effects of Ser16 Phosphorylation on the Allosteric Transitions of phospholamban/Ca^{2+}-ATPase Complex, *J. Mol. Biol. 358*, 1041−1050.
27. Kimura, Y., Kurzydlowski, K., Tada, M., and MacLennan, D. H. (1997) Phospholamban Inhibitory Function is Activated by Depolymerization, *J. Biol. Chem. 272*, 15061−15064.
28. Reddy, L. G., Jones, L. R., and Thomas, D. D. (1999) Depolymerization of Phospholamban in the Presence of Calcium Pump: A Fluorescence Energy Transfer Study, *Biochemistry 38*, 3954−3962.
29. Zamoon, J., Mascioni, A., Thomas, D. D., and Veglia, G. (2003) NMR Solution Structure and Topological Orientation of Monomeric Phospholamban in Dodecylphosphocholine Micelles, *Biophys. J. 85*, 2589−2598.
30. Pollesello, P., Annila, A., and Ovaska, M. (1999) Structure of the 1−36 Amino-Terminal Fragment of Human Phospholamban by Nuclear Magnetic Resonance and Modeling of the Phospholamban Pentamer, *Biophys. J. 76*, 1784−1795.
31. Lambeth, S., Schmid, H., Muenchbach, M., Vorherr, T., Krebs, J., Carafoli, E., and Griesinger, C. (2000) NMR Solution Structure of Phospholamban, *Helv. Chim. Acta 83*, 2141−2152.
32. Metcalfe, E. E., Zamoon, J., Thomas, D. D., and Veglia, G. (2004) $^{1}H/^{15}N$ Heteronuclear NMR Spectroscopy shows Four Dynamic Domains for Phospholamban Reconstituted in Dodecylphosphocholine Micelles, *Biophys. J. 87*, 1205−1214.
33. Metcalfe, E. E., Traaseth, N. J., and Veglia, G. (2005) Serine 16 Phosphorylation Induces an Order-to-Disorder Transition in Monomeric Phospholamban, *Biochemistry 44*, 4386−4396.
34. Schmidt, A. G., Zhai, J., Carr, A. N., Gerst, M. J., Lorenz, J. N., Pollesello, P., Annila, A., Hoit, B. D., and Kranias, E. G. (2002) Structural and Functional Implications of the Phospholamban Hinge Domain: Impaired SR Ca^{2+} Uptake as a Primary Cause of Heart Failure, *Cardiovasc. Res. 56*, 248−259.
35. Oxenoid, K., and Chou, J. J. (2005) The Structure of Phospholamban Pentamer Reveals a Channel-Like Architecture in Membranes, *Proc. Natl. Acad. Sci. U.S.A. 102*, 10870−10875.
36. Traaseth, N. T., Verardi, R., Torgersen, K. D., Karim, C. B., Thomas, D. D., and Veglia, G. (2007) Spectroscopic Validation of the Pentameric Structure of Phospholamban, *Proc. Natl. Acad. Sci. U.S.A. 104*, 14676−14681.
37. Mascioni, A., Karim, C., Barany, G., Thomas, D. D., and Veglia, G. (2002) Structure and Orientation of Sarcolipin in Lipid Environments, *Biochemistry 41*, 475−482.
38. Opella, S. J. (1997) NMR and Membrane Proteins, *Nat. Struct. Biol. 4* (Suppl.), 845−848.
39. Baldus, M. (2006) Molecular Interactions Investigated by Multi-Dimensional Solid-State NMR, *Curr. Opin. Struct. Biol. 16*, 618−623.
40. Mascioni, A., Karim, C., Zamoon, J., Thomas, D. D., and Veglia, G. (2002) Solid-State NMR and Rigid Body Molecular Dynamics to Determine Domain Orientations of Monomeric Phospholamban, *J. Am. Chem. Soc. 124*, 9392−9393.
41. Wu, C. H., Ramamoorthy, A., and Opella, S. J. (1994) High-Resolution Heteronuclear Dipolar Solid-State NMR Spectroscopy, *J. Magn. Reson. 109*, 270−272.
42. Traaseth, N. J., Buffy, J. J., Zamoon, J., and Veglia, G. (2006) Structural Dynamics and Topology of Phospholamban in Oriented Lipid Bilayers using Multidimensional Solid-State NMR, *Biochemistry 45*, 13827−13834.
43. Grage, S. L., Wang, J., Cross, T. A., and Ulrich, A. S. (2002) Solid-State ^{19}F-NMR Analysis of ^{19}F-Labeled Tryptophan in Gramicidin A in Oriented Membranes, *Biophys. J. 83*, 3336−3350.
44. Aisenbrey, C., and Bechinger, B. (2004) Investigations of Polypeptide Rotational Diffusion in Aligned Membranes by ^{2}H and ^{15}N Solid-State NMR Spectroscopy, *J. Am. Chem. Soc. 126*, 16676−16683.
45. Park, S. H., Mrse, A. A., Nevzorov, A. A., De Angelis, A. A., and Opella, S. J. (2006) Rotational Diffusion of Membrane Proteins in Aligned Phospholipid Bilayers by Solid-State NMR Spectroscopy, *J. Magn. Reson. 178*, 162−165.
46. Andronesi, O. C., Becker, S., Seidel, K., Heise, H., Young, H. S., and Baldus, M. (2005) Determination of Membrane Protein Structure and Dynamics by Magic-Angle-Spinning Solid-State NMR Spectroscopy, *J. Am. Chem. Soc. 127*, 12965−12974.
47. Hughes, E., Clayton, J. C., and Middleton, D. A. (2005) Probing the Oligomeric State of Phospholamban Variants in Phospholipid Bilayers from Solid-State NMR Measurements of Rotational Diffusion Rates, *Biochemistry 44*, 4055−4066.
48. Karp, E. S., Tiburu, E. K., Abu-Baker, S., and Lorigan, G. A. (2006) The Structural Properties of the Transmembrane Segment of the Integral Membrane Protein Phospholamban Utilizing ^{13}C CPMAS, ^{2}H, and REDOR Solid-State NMR Spectroscopy, *Biochim. Biophys. Acta 1758*, 772−780.
49. Buffy, J. J., Traaseth, N. J., Mascioni, A., Gor'kov, P. L., Chekmenev, E. Y., Brey, W. W., and Veglia, G. (2006) Two-Dimensional Solid-State NMR Reveals Two Topologies of Sarcolipin in Oriented Lipid Bilayers, *Biochemistry 45*, 10939−10946.
50. Stokes, D. L., Pomfret, A. J., Rice, W. J., Glaves, J. P., and Young, H. S. (2006) Interactions between Ca^{2+}-ATPase and the Pentameric Form of Phospholamban in Two-Dimensional Co-Crystals, *Biophys. J. 90*, 4213−4223.
51. Tatulian, S. A., Jones, L. R., Reddy, L. G., Stokes, D. L., and Tamm, L. K. (1995) Secondary Structure and Orientation of Phospholamban Reconstituted in Supported Bilayers from Polarized Attenuated Total Reflection FTIR Spectroscopy, *Biochemistry 34*, 4448−4456.
52. Arkin, I. T., Rothman, M., Ludlam, C. F., Aimoto, S., Engelman, D. M., Rothschild, K. J., and Smith, S. O. (1995) Structural Model of the Phospholamban Ion Channel Complex in Phospholipid Membranes, *J. Mol. Biol. 248*, 824−834.
53. Smith, S. O., Kawakami, T., Liu, W., Ziliox, M., and Aimoto, S. (2001) Helical Structure of Phospholamban in Membrane Bilayers, *J. Mol. Biol. 313*, 1139−1148.
54. Robia, S. L., Flohr, N. C., and Thomas, D. D. (2005) Phospholamban Pentamer Quaternary Conformation Determined by in-Gel Fluorescence Anisotropy, *Biochemistry 44*, 4302−4311.
55. Simmerman, H. K., Kobayashi, Y. M., Autry, J. M., and Jones, L. R. (1996) A Leucine Zipper Stabilizes the Pentameric Membrane Domain of Phospholamban and Forms a Coiled-Coil Pore Structure, *J. Biol. Chem. 271*, 5941−5946.

56. Karim, C. B., Stamm, J. D., Karim, J., Jones, L. R., and Thomas, D. D. (1998) Cysteine Reactivity and Oligomeric Structures of Phospholamban and its Mutants, *Biochemistry 37*, 12074−12081.
57. Zamoon, J., Nitu, F., Karim, C., Thomas, D. D., and Veglia, G. (2005) Mapping the Interaction Surface of a Membrane Protein: Unveiling the Conformational Switch of Phospholamban in Calcium Pump Regulation, *Proc. Natl. Acad. Sci. U.S.A. 102*, 4747−4752.
58. Karim, C. B., Kirby, T. L., Zhang, Z., Nesmelov, Y., and Thomas, D. D. (2004) Phospholamban Structural Dynamics in Lipid Bilayers Probed by a Spin Label Rigidly Coupled to the Peptide Backbone, *Proc. Natl. Acad. Sci. U.S.A. 101*, 14437−14442.
59. Wagner, G., Pardi, A., and Wuthrich, K. (1983) Hydrogen Bond Length and Proton NMR Chemical Shifts in Proteins, *J. Am. Chem. Soc. 105*, 5948−5949.
60. Kimura, Y., Asahi, M., Kurzydlowski, K., Tada, M., and MacLennan, D. H. (1998) Phospholamban Domain Ib Mutations Influence Functional Interactions with the Ca^{2+}-ATPase Isoform of Cardiac Sarcoplasmic Reticulum, *J. Biol. Chem. 273*, 14238−14241.
61. Inesi, G., Lewis, D., Ma, H., Prasad, A., and Toyoshima, C. (2006) Concerted Conformational Effects of Ca^{2+} and ATP are Required for Activation of Sequential Reactions in the Ca^{2+} ATPase (SERCA) Catalytic Cycle, *Biochemistry 45*, 13769−13778.
62. Ha, K. N., Traaseth, N. J., Verardi, R., Zamoon, J., Cembran, A., Karim, C. B., Thomas, D. D., Veglia, G. (2007) Controlling the Inhibition of the Sarcoplasmic Ca2+-ATPase by Tuning Phospholamban Structural Dynamics, *J. Biol. Chem.* E-pub Sep. 30, 2007.

BI701668V